ICANS-XIV
14th Meeting of the International Collaboration on
Advanced Neutron Sources
June 14-19, 1998
Argonne National Laboratory, 9700 S. Cass Avenue, Argonne, IL 60439, USA

Measurements of Reaction Rate Distributions on a Mercury Target Bombarded with High Energy Protons

H.Takada, Y.Kasugai, H.Nakashima, Y.Ikeda, Y.Oyama, N.Watanabe, M.Arai*,
Y.Kiyanagi** and ASTE Collaboration

Center for Neutron Science
Japan Atomic Energy Research Institute,
Tokai-mura, Naka-gun, Ibaraki-ken, 319-1195, JAPAN

*: High Energy Accelerator Research Organization,
Oho, Tsukuba-shi, Ibaraki-ken, 305-8581, JAPAN

**: Faculty of Engineering, Hokkaido University,
Kita-13, Nishi-8, Kita-ku, Sapporo, 060-8628, JAPAN

Abstract

A spallation target experiment under the ASTE collaboration was carried out using a thick mercury target bombarded by 1.5 to 24 GeV protons. Reaction rate distributions on the target were measured using various activation detectors at incident proton energies of 1.5, 7.0 and 24.0 GeV. The intensity distribution of leakage neutrons was estimated from the measured reaction rate data of the $^{115}In(n,n')^{115m}In$ reaction. In consequence, the intensity distribution had a peak at 11.5 cm from the top of hemisphere of the mercury target for 1.5 GeV proton incidence and the peak position moved to 16.1 cm for 7.0 GeV and 19.6 cm for 24.0 GeV respectively. It was also found that the calculations using Monte Carlo code systems reproduced the measured reaction rate distributions qualitatively well.

1. Introduction

An international collaboration on a spallation target experiment at the Alternating Gradient Synchrotron (AGS) of Brookhaven National Laboratory (BNL), namely ASTE collaboration, was organized. Main missions are to study the neutronic, thermal and mechanical characteristics of a mercury target for estimating its feasibility as the spallation target because mercury has been proposed for one of the most promising target materials for an intense spallation neutron source driven by the proton accelerator with a power of 5 MW.

The experimental data related to the production and transport of spallation neutrons in the thick mercury target are important neutronics characteristics because of lack of experiments associated with the mercury target at incident energies above 1 GeV. They are also useful for the validation of calculation codes for the neutronic design study, such as HERMES[1], LAHET[2] and NMTC/JAERI[3].

Keywords : Mercury target, Reaction rate distribution, 1.5, 7.0 and 24.0 GeV protons

Under the ASTE collaboration, the reaction rate distributions on the mercury target have been measured using various activation detectors with different threshold energies. The three kind of incident energies of 1.5, 7.0 and 24.0 GeV were chosen as the incident proton energies according to the interest for the future plans of the spallation neutron source development.

2. Experimental

2.1 Activation Detector Arrangement

The mercury target was installed at a target room of the U-line of the AGS facility. The target configuration was 20 cm diameter and 130 cm long cylinder having the hemispherical top surface. Figure 1 shows the cross sectional view of the mercury target. The activation detectors were put on an acrylic bar and then installed on the four radial positions along the beam axis with an interval of 90° around the target. The position of 45° right-hand upward toward the downstream of the beam axis was indexed as "Main" and the others were labeled as "Sub-1", "Sub-2" and "Sub-3" according to the counter clockwise rotation direction around the target, respectively.

The following high purity metal foils were employed as activation detectors : In, Nb, Al, Au, Bi, Co, Ni, Fe and Cu. The size and purity of the foils are summarized in Table 1. The foils were classified into the following three groups: (A) In, (B) Nb, Al, Au and Bi, (C) Co, Ni, Fe and Cu. The foils classified into (B) and (C) were assembled to one foil stack, respectively, and then put on the acrylic bar. The In foils were set on the 17 positions from 0.5 to 95 cm on the "Main" position to obtain a neutron flux profile along the target, while the other foil stacks were mounted on 6 positions.

The physical characteristics of the activation detectors are listed in Table 2. The detectors cover from 0.5 to 54.0 MeV in threshold energy. The neutron cross sections of some detectors are shown in Fig. 2, where the cross section values below 20 MeV were taken from JENDL-Dosimetry file[4] and those above 20 MeV were calculated with the ALICE-F code[5].

2.2 γ-ray measurement

The γ-ray spectra of the activated foils were measured using the same Ge-detectors and data acquisition system for the beam characteristics measurement[6]. At each proton irradiation campaign, a series of γ-ray measurements for short-lived radioactivities was continued for 10 to 12 hours including the time needed to the foil sorting. Second measurements for modest long half-lived nuclides were performed a few days after irradiation.

The reaction rate of individual activation detector was obtained from the peak counts by correcting such as the decay, the detector efficiency, the coincidence sum effect in counting, the γ-ray self-absorption effect in foil and so on. The physical constants such as decay constant and branching ratio were taken from Ref. 7. The detector efficiency was determined by a γ-ray measurement using calibrated radioactive standard sources.

In this measurement, the sources of error in the data processing was attributed to the following items: 1) statistical error of peak count, 2) detector efficiency error, 3) uncertainty of the number of incident protons, 4) error of the weight of foil. The statistical error of peak count was better than 10 % in most cases for the activation detectors listed in Table 2. The detector efficiency error was estimated as 2.0 % from the calibration measurement with standard sources. The uncertainty of the number of incident protons was taken from the results[6] of the activation technique using the $Cu(p,x)^{24}Na$ reaction. The error of the weight of foil stack was less than 0.1 %. The errors concerning to the decay constant, γ-ray branching ratio, irradiation time, measuring time, cooling time were negligible small.

3. Calculations

The calculations were performed with the NMTC/JAERI-MCNP4A[8] code system. NMTC/JAERI simulates the nuclear reactions and particle transport in the energy region above 20 MeV by the use of the intranuclear cascade model of Bertini [9], the preequilibrium calculation model of Yoshizawa et al.[10] and a particle evaporation model taking account of the high energy fission process. The level density parameter derived by a formulae of Ignatyuk [11] was used in the evaporation calculation. The cut off energies for particle transport were set to be 20 MeV for neutron and 2 MeV for charged particles. The neutron flux on the cylindrical surface of the mercury target was estimated with the energy group structure defined in the HILO-86R library [12] up to 400 MeV. For neutrons above 400 MeV, For neutrons above 400 MeV, the energy group structure was extended up to 1.5 GeV. The reaction rate was obtained using the nuclide production cross section values calculated by the ALICE-F code. Here, some of calculated cross sections were adjusted to connect smoothly with the ones compiled in JENDL Dosimetry file at 20 MeV.

MCNP4A calculates the transport of the neutrons in the energy region lower than 20 MeV using a continuous energy cross section library which has been processed from JENDL-Fusion File [13].

The applicable energy range of the NMTC/JAERI code is limited up to 3.5 GeV for nucleons. The analyses for 7.0 and 24.0 GeV proton incidence have been carried out using the HERMES code system[1]. The nuclear data library and nuclide production cross sections used in the HERMES code system were the same as those for the NMTC/JAERI-MCNP4A calculation.

As reported in the incident proton beam characteristics measurement[6], the beam center was shifted from the target center. This condition was treated in the geometry model of the calculation as follows: The mercury target has the radius equal to the distance from the measured beam center position to the position of individual acrylic bar. The shape of incident beam was given by the fitting of the measured beam profile[6] with Gaussian distribution.

4. Results and Discussion

The reaction rate distribution of the $^{115}In(n,n')^{115m}In$ reaction measured on the "Main" position is shown in Fig 3 with those on the other positions for 1.5 GeV proton incidence on the mercury target. It is observed that the reaction rate values among the four positions differ from each other because the beam incident position shifted from the center axis of the target. The difference of about 50 % is observed in the reaction rates between the "Main" position and the "Sub-1" one at the distance range of 9 to 25 cm. The similar results were observed even in the cases of 7.0 and 24.0 GeV proton incidence, respectively, although they are not presented in this paper.

Figure 4 shows the reaction rate distributions of the $^{115}In(n,n')^{115m}In$ reaction on the cylindrical surface of the mercury target for 1.5, 7.0 and 24.0 GeV. In this case, the measured reaction rates were normalized to the values estimated by the NMTC/JAERI-MCNP4A calculation with the assumption that the proton beam was incident on the center of mercury target with radius of 10 cm. The peak position, full-width-half-maximum (FWHM) of peak and the attenuation constant were obtained from the normalized data by a curve fit. The results are summarized in Table 3. It is found that the peak position of reaction rate distribution moves to deeper positions along the mercury target with increase of incident proton energy. The peak position lies on 11.5 cm from the top of hemisphere of the mercury target for 1.5 GeV proton incidence, while it moves to 16.1 cm for 7.0 GeV and 19.6 cm for 24.0 GeV, respectively. In addition, the higher the incident energy becomes, the shorter the attenuation constant of the reaction rate distribution becomes. This is the evident that the number of neutrons transported

to the deeper position of the mercury target increases with incident proton energy. The measured data can be regarded as the neutron yield distribution along the mercury target because the $^{115}In(n,n')^{115m}In$ reaction has the threshold of 0.4 MeV enough to be sensitive to most of energetic neutrons.

The reaction rate distribution of the $^{92}Nb(n,2n)^{92m}Nb$ reaction measured along the mercury target is shown in Fig. 5. The reaction rate rises up from the front surface to the peak position, and then decreases with the distance. The peak position moves to deeper position from the front surface with increase of incident energy as well as the results of the $^{115}In(n, n')^{115m}In$ reaction.

In order to study the characteristics of the reaction rate distributions dependent on activation detectors and incident proton energy, the measured data of the different reactions of $^{115}In(n,n')^{115m}In$, $^{92}Nb(n,2n)^{92m}Nb$ and $^{209}Bi(n, 6n)^{204}Bi$ are compared in Fig. 6. For comparison, the measured data were normalized to those for 1.5 GeV proton incidence at all positions along the mercury target. It is observed that the reaction rate ratios among the three reactions increases with the distance from the front surface. In addition, the gradient of the reaction rate ratios for 24.0 GeV are steeper than those for 7.0 GeV. These results indicate that the spallation neutrons have been produced and transported in broader space in the mercury target with increase of the incident proton energy. On the other hand, there is little difference among the reaction rate ratios in case of the same incident energy. Thus, the shape of the reaction rate distribution is insensitive to the threshold energy of the activation detector.

The results of the NMTC/JAERI-MCNP4A calculations are compared with the experiments in Figs. 7(a) to 10 for 1.5 GeV proton incidence on the mercury target. Figures 8(a) and 8(b) show the results of the HERMES calculation with the experiments for 24.0 GeV proton incidence. For the $^{115}In(n,n')^{115m}In$ reaction, the NMTC/JAERI-MCNP4A calculation gives about 20% higher reaction rates than the experiments although the calculation reproduces the relative difference of reaction rates at different radial positions with respect to the "Main" position. As shown in Fig. 8(a), on the other hand, a large disagreement of about a factor of 2 is observed between the HERMES calculation and the experiment for 24 GeV. In HERMES, nuclear reaction is simulated with the physics models applicable below 3.5 GeV with an extrapolated nuclear data. The treatment of many other elemental interactions between intranuclear particles are missing in the code. This approximation may be too crude to reproduce the measured reaction rates. However, it is reported[14] that the code system could predicts well the total neutron yield of a thick lead target bombarded with protons below 12 GeV. This is a contradictory conclusion against the present result shown in Fig. 8(a). In the present calculation, the neutron yield in the energy region sensitive to the $^{115}In(n,n')^{115m}In$ reaction may be enhanced by some reason. The certain reason cannot be found in this work for the time being. More detailed investigation is required for both the data processing and analytical procedure to discuss about the source of disagreement.

As shown in Figs. 9 and 10, the NMTC/JAERI-MCNP4A calculations reproduce well the shape of reaction rate distributions of the activation detectors with higher threshold energies for 1.5 GeV proton incidence. However, significant disagreement is observed between the calculations and experiments at the positions near the beam incident surface. This is outstanding in the results of the $^{209}Bi(n,xn)$ reactions. The incident beam hits upon curving surface of the hemisphere part of the mercury target with broad profile. In the calcualtion, on the other hand, the proton beam was assumed to be injected on the top of the hemisphere part. The slight difference of target geometry between the calculation and the experiment may affect the neutron yield at the vicinity of the incident point so that the calculation estimates the neutron yield lower than the experiment. It is also noted that the calculated reaction rate values of the activation detectors with high threshold energies include the ambiguities because the neutron

cross sections calculated with ALICE-F code have not been evaluated. This is a subject to be solved to estimate the accuracy of the calculation code system in the analysis of thick target experiments.

5. Conclusions

The neutron intensity distribution along the cylindrical surface of the mercury target was estimated using the activation detector of the $^{115}In(n,n')^{115m}In$ reaction for 1.5, 7.0 and 24.0 GeV proton energies. It was found that the distribution of the leakage neutrons had a peak and the peak position moved to deeper position along the mercury target with increase of incident energy. The peak position lies on 11.5 cm from the top of hemisphere of the mercury target for 1.5 GeV proton incidence, while it is located on 16.1 and 19.6 cm for 7.0 and 24.0 GeV one, respectively.

The reaction rate distributions of various other activation detectors were also measured on the cylindrical surface of the mercury target. It was found that the distributions had relatively the same shape as that of the $^{115}In(n,n')^{115m}In$ reaction. These data would be useful for estimating the neutron flux distribution. Judging from the results analyzed up to now, the fine energy spectrum could be obtained by unfolding procedure in the energy range from 0.5 to 54 MeV.

The measured data were compared with the calculations uisng Monte Carlo code systems of NMTC/JAERI-MCNP4A and HERMES with the nuclide production cross section values combining the JENDL dosimetry file with the ALICE-F calculation. It was found that the calculations reproduce the measured reaction rate distributions qualitatively well. However, some disagreement appeared between the calculations and experiments for the activation detectors sensitive to neutrons above 20 MeV. The disagreement became more significant for 24.0 GeV proton incidence than for 1.5 GeV. This is attributable to the fact that the neutron cross section values in this energy range has not been verified. Further study is required from both of experimental and analytical point of view to remove the disagreement.

References

[1] P.Cloth, et al.: "HERMES A Monte Carlo Program System for Beam Materials Interaction Studies", Jül-2203, (1988).

[2] R.E.Prael, H.Lichtenstein : LA-UR-89-3014, "Users Guide to LCS: The LAHET Code System", (1989).

[3] Y.Nakahara, T.Tsutsui: "NMTC/JAERI A Code System for High Energy Nuclear Reactions and Nucleon-Meson Transport Code", JAERI-M 82-198 (1982), [in Japanese].; H.Takada, et al.: "An Upgraded Version of the Nucleon-Meson Transport Code NMTC/JAERI97", JAERI-Data/Code 98-005 (1998).

[4] M.Nakazawa, et al. : "JENDL Dosimetry File", JAERI-1325, (1992).

[5] T.Fukahori :"ALICE-F Calculation of Nuclear Data up to 1 GeV", Proc. of the Specialists' Mtg. on High Energy Nucl. Data, Oct. 3-4, 1991, JAERI, Tokai, JAERI-M 92-039, pp. 114-122 (1992).

[6] H.Nakashima, , et al. : "Measurement of Incident Proton Beam Characteristics for AGS Spallation Experiment", This Proceedings.

[7] C.M.Lederer and V.S.Shirley (Ed.): "Table of Isotopes 7th Edition", Willey Interscience Publication, N.Y., (1978).

[8] J.F.Briesmeister (Ed.) : "MCNP A General Monte Carlo N-Particle Transport Code, Version 4A", LA-12625, (1993).

[9] H.W.Bertini : Phys. Rev. **188**, (1969) 1711.

[10] N.Yoshizawa, K.Ishibashi, H.Takada : J. Nucl. Sci. Technol. **32**, (1995) 601.
[11] A.V.Ignatyuk, G.N.Smirenkin, A.S.Tishin : Sov. J. Nucl. Phys. **21** (1975) 256 .
[12] H.Kotegawa, Y.Nakane, A.Hasegawa, Sh.Tanaka :"Neutron-photon Multigroup Cross Sections for Neutron Energies up to 400 MeV; HILO86R", JAERI-M 93-020, (1993).
[13] S.Chiba, B.Yu, T.Fukahori : "Evaluation of JENDL Fusion File", Proc. of the 1991 Symp. on Nucl. Data, Nov. 28-29, 1991, JAERI, Tokai, Japan, JAERI-M 92-027, pp. 35-44 (1992).
[14] M.Arai, et al.: "Study on Neutron Yield for 12 GeV Protons", Proc. of the 3rd Workshop on Simulating Accel. Radiat. Environments (SARE3), May 7-9, 1997, KEK, tsukuba, Japan, KEK Proceedings 97-5, 293 (1997).

Table 1. Physical characteristics of foils employed as activation detectors.

Foil	Size	Purity
In	18 x 20 x 1.0 mm	99.99 %
	18 x 20 x 0.1 mm	
Al	20 x 20 x 1.0 mm	99.99 %
Nb	20 x 20 x 1.0 mm	99.95 %
Au	20 x 20 x 0.2 mm	99.95 %
Bi	20 ϕ x 2 mm	99.998 %
	15 ϕ x 1.5 mm	
Co	20 x 20 x 1 mm	99.9 %
Fe	20 x 20 x 1 mm	99.9 %
Ni	20 x 20 x 1 mm	99.9 %
Cu	20 x 20 x 1 mm	99.99 %

Table 2. Nuclear characteristics of activation detectors.

Activation Detector	Half Life	γ-ray Energy	Branching Ratio	Threshold
$^{115}In(n,n')^{115m}In$	4.3 hr	336.24 keV	46.7 %	0.5 MeV
$^{27}Al(n,x)^{24}Na$	15.02 hr	1368.9 keV	100%	4.9 MeV
$^{93}Nb(n,2n)^{92m}Nb$	10.12 day	934.46 keV	99.15 %	8.9 MeV
$^{93}Nb(n,4n)^{90}Nb$	14.7 hr	1129.2 keV	92.7 %	29.1 MeV
$^{197}Au(n,2n)^{196}Au$	6.183 day	355.65 keV	87.7 %	8.1 MeV
$^{197}Au(n,2n)^{196m}Au$	9.7 hr	147.77 keV	61.3%	8.7 MeV
$^{197}Au(n,4n)^{194}Au$	39.5 hr	328.47 keV	43.0%	23.2 MeV
$^{197}Au(n,\gamma)^{198}Au$	2.696 day	411.8 keV	95.5%	-
$^{209}Bi(n,4n)^{206}Bi$	6.243 day	803.1 keV	98.9%	22.6 MeV
$^{209}Bi(n,5n)^{205}Bi$	15.31 day	703.5 keV	31.0%	29.6 MeV
$^{209}Bi(n,6n)^{204}Bi$	11.3 hr	899.2 keV	99.2%	38.0 MeV
$^{209}Bi(n,7n)^{203}Bi$	11.76hr	820.3 keV	29.6%	45.3 MeV
$^{209}Bi(n,8n)^{202}Bi$	1.67 hr	422.2 keV	83.8%	54.0 MeV

Table 3. Characteristics of measured reaction rate distributions of the $^{115}In(n,n')^{115m}In$ reaction.

Incident Energy	Peak Position	FWHM of Peak	Attenuation constant after peak
1.5 GeV	11.5 cm	29.2 cm	0.0724
7.0 GeV	16.1 cm	38.2 cm	0.0498
24.0 GeV	19.6 cm	44.2 cm	0.0407

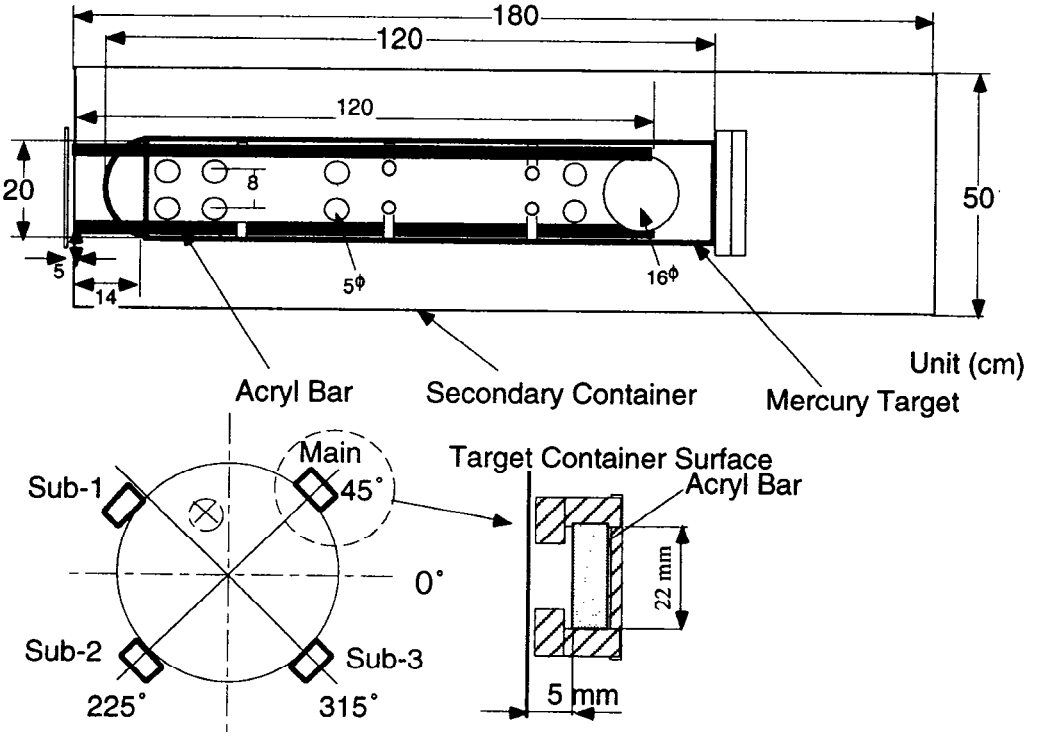

Fig.1 Cross sectional view of the mercury target.

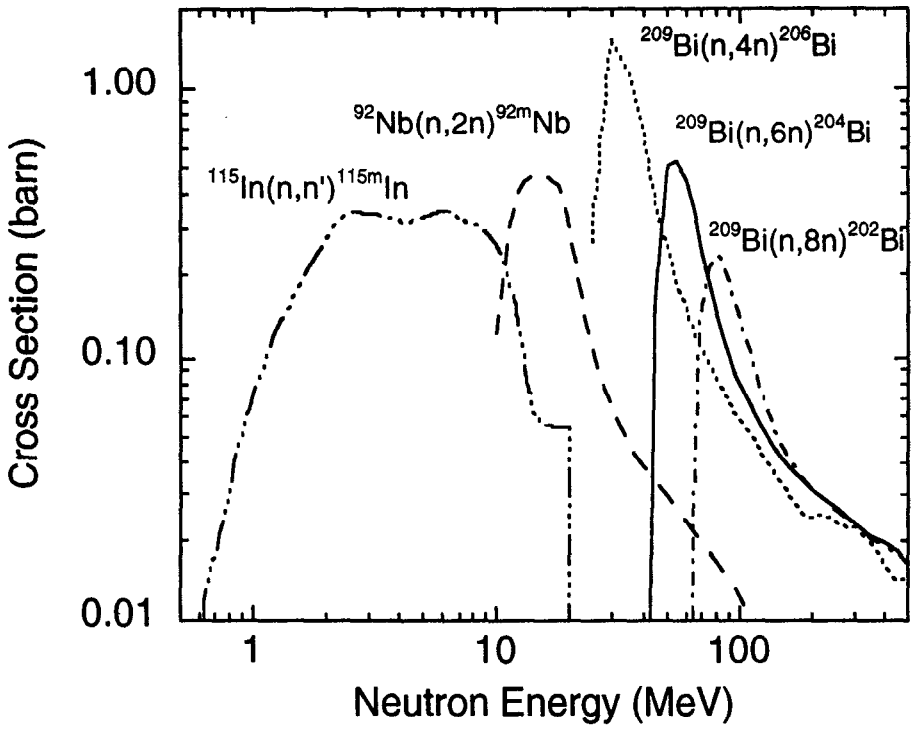

Fig. 2 Neutron cross sections of the reactions of ^{115}In(n,n')^{115m}In, ^{93}Nb(n,2n)^{92m}Nb, ^{209}Bi(n,4n)^{206}Bi, ^{209}Bi(n,6n)^{204}Bi and ^{209}Bi(n,8n)^{202}Bi.

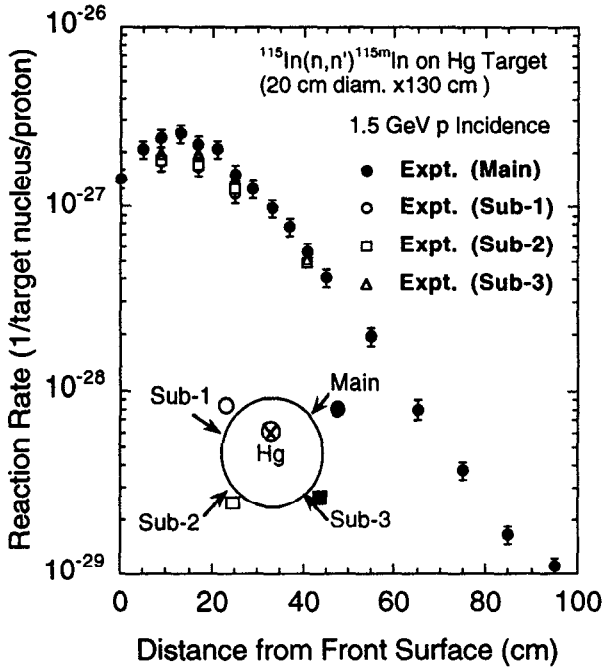

Fig. 3 Reaction rate distribution of the ^{115}In (n,n')^{115m}In reaction measured on the mercury target bombarded with 1.5 GeV proton incidence.

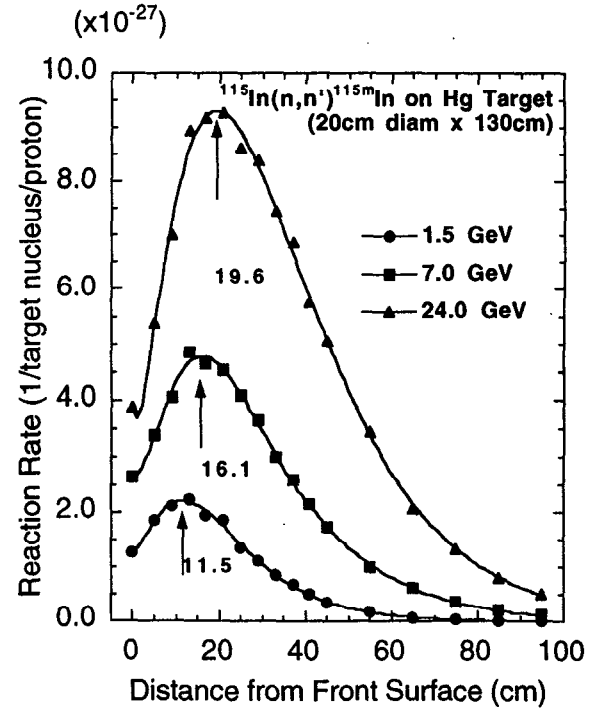

Fig. 4 Comparison of reaction rate distributions of the ^{115}In (n,n')^{115m}In reaction measured on the mercury target bombarded with protons of 1.5, 7.0 and 24.0 GeV.

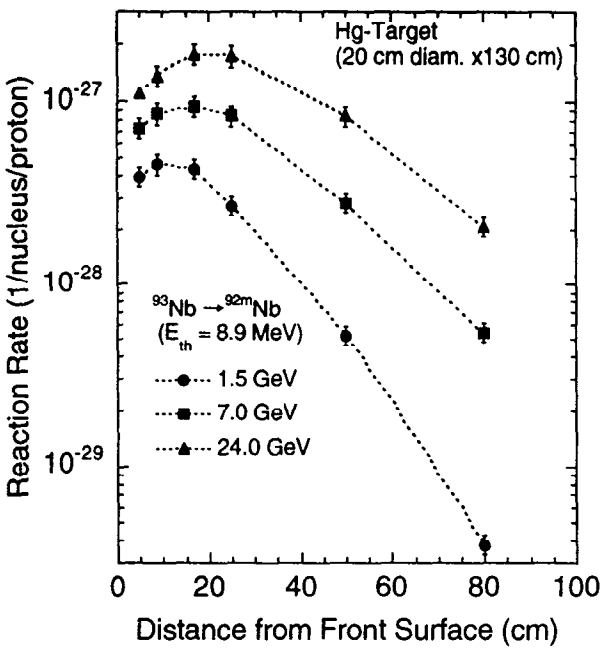

Fig. 5 Reaction rate distributions of the ^{92}Nb (n,2n)^{92m}Nb reaction measured on the mercury target bombarded with protons of 1.5, 7.0 and 24.0 GeV.

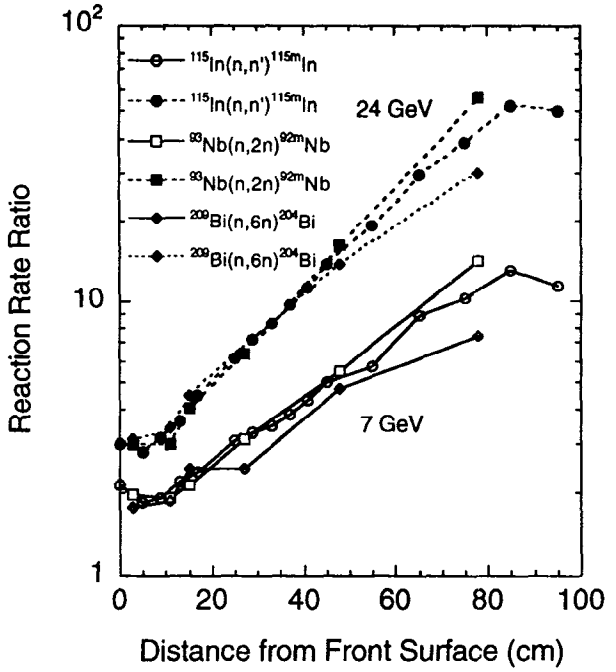

Fig. 6 Measured reaction rate ratios of the reactions of ^{115}In (n,n')^{115m}In, ^{92}Nb (n,2n)^{92m}Nb and ^{209}Bi (n,6n))^{204}Bi for 7.0 and 24.0 GeV proton incidence on the mercury target to those for 1.5 GeV one.

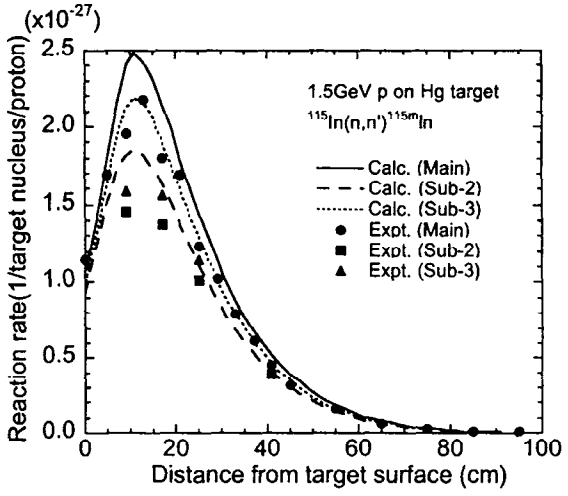

Fig. 7(a) Comparison of calculated and experimental reaction rates of the ^{115}In (n,n')^{115m}In reaction for 1.5 GeV proton incidence on the mercury target. The solid marks indicate the experimental results. The lines stand for the calculated results of NMTC/JAERI-MCNP4A.

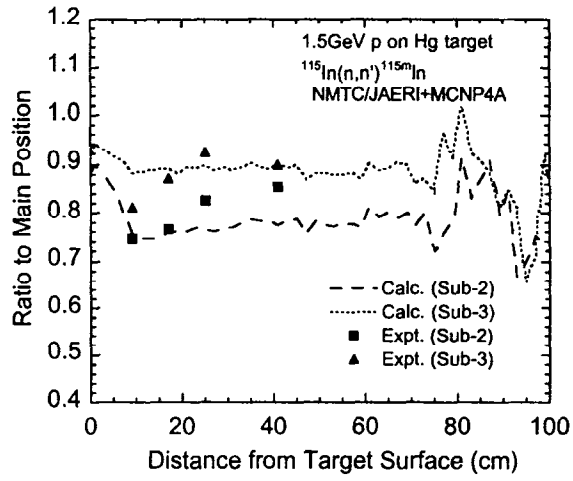

Fig. 7(b) Ratios of the reaction rates of ^{115}In (n,n')^{115m}In at different radial positions to those at the "Main" position. The notes to the marks and the lines are the same as for Fig. 7(a).

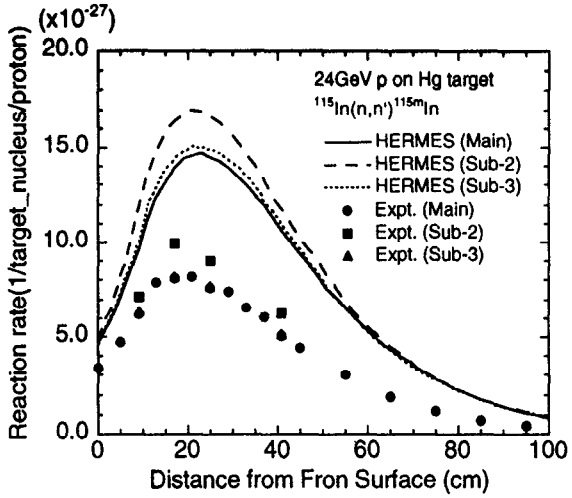

Fig. 8(a) Comparison of calculated and experimental reaction rates of the ^{115}In (n,n')^{115m}In reaction for 24.0 GeV proton incidence on the mercury target. The notes to the marks and the lines are the same as for Fig. 7(a).

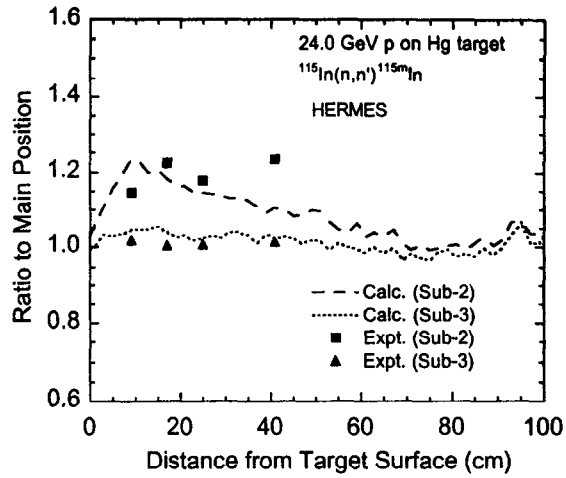

Fig. 8(b) Ratios of the reaction rates of the ^{115}In (n,n')^{115m}In reaction at the different radial positions to those at the "Main" position. The notes to the marks and the lines are the same as for Fig. 7(a).

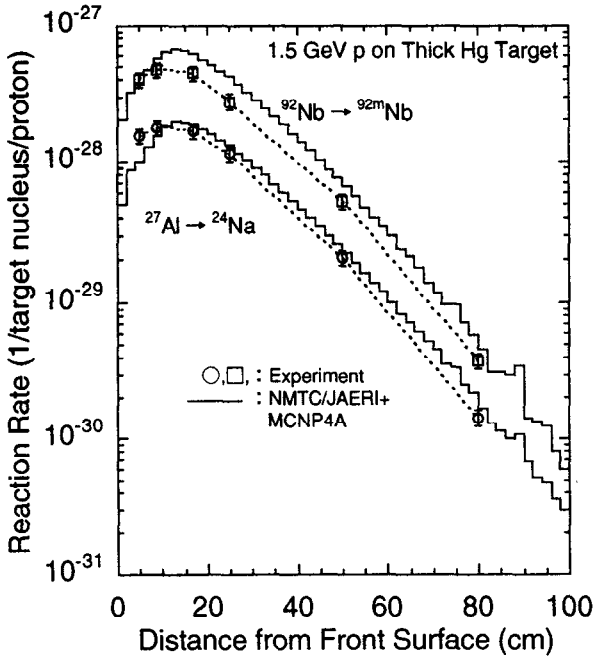

Fig. 9 Comparison of calculations with experiments for the reactions of ^{27}Al(n,x)^{24}Na and ^{93}Nb(n,2n)^{92m}Nb for 1.5 GeV proton incidence on the mercury target. The open marks indicate the experimental results. The solid lines stand for the calculated results of the NMTC/JAERI-MCNP4A code system. The dotted lines are for eye-guide.

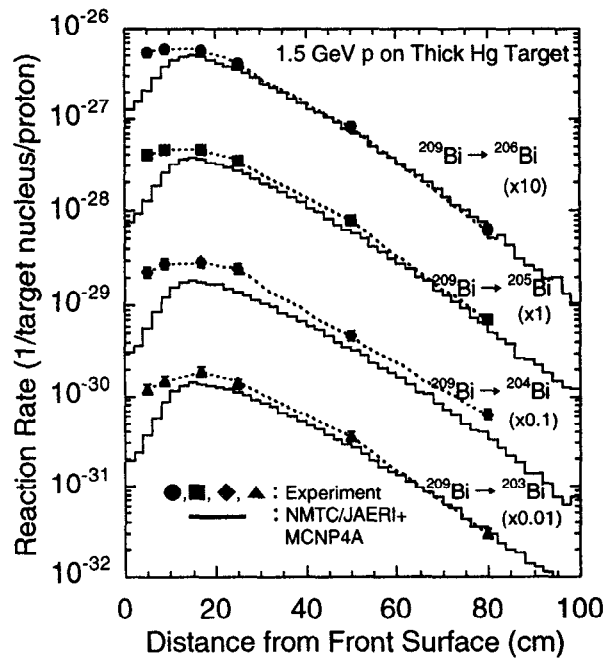

Fig. 10 Comparison of calculations with experiments for the reaction rates of ^{209}Bi(n,xn) for 1.5 GeV proton incidence on the mercury target. The notes to the marks and the lines are the same as for Fig. 9.